J Mater Sci (2014) 49:5208–5217
DOI 10.1007/s10853-014-8230-3

Electronic band structure and optoelectronic properties of $SrCu_2X_2$ (X = As, Sb): DFT calculation

Saleem Ayaz Khan · A. H. Reshak · Z. A. Alahmed

Received: 11 February 2014 / Accepted: 5 April 2014 / Published online: 23 April 2014

Abstract All-electron-full potential linear-augmented plane wave method with Engel Vosko approximation was used for calculating the electronic structure, Fermi surface, and optical properties of $SrCu_2X_2$ (X = As, Sb). The calculated band structure and Fermi surface show that the metallic behavior of $SrCu_2X_2$ increases as one move from As to Sb. The calculated partial density of states shows that As-s/p/d, Cu-s/p, and Sr-s/p/d states are forming the Fermi surface for $SrCu_2As_2$, whereas Sb-s/p/d, Cu-s/p, and Sr-s/p/d states are forming the Fermi surface for $SrCu_2Sb_2$. The calculated densities of states at Fermi level and electronic specific heat are 14.2 (42.57) states/Ryd-cell and 2.60 (7.37) mJ/mol K^2 for $SrCu_2As_2$ ($SrCu_2Sb_2$). The complex optical dielectric function's dispersion and the related optical properties such as refractive indices, extension coefficient, absorption coefficient, reflectivity, energy loss function, and optical conductivity were calculated and discussed in detail. The optical properties show a considerable anisotropy between the two components.

S. A. Khan (✉) · A. H. Reshak
New Technologies - Research Center, University of West Bohemia, Univerzitni 8, 306 14 Pilsen, Czech Republic
e-mail: sayaz_usb@yahoo.com

A. H. Reshak
e-mail: maalidph@yahoo.co.uk

A. H. Reshak
Center of Excellence Geopolymer and Green Technology, School of Material Engineering, University Malaysia Perlis, 01007 Kangar, Perlis, Malaysia

Z. A. Alahmed
Department of Physics and Astronomy, King Saud University, Riyadh 11451, Saudi Arabia

Introduction

The investigation of novel high-temperature superconductors and its mechanism are always highlighted in condensed matter physics [1]. Among them, the AB_2M_2-type crystals are considered to have the largest family members of the crystals [2]. In AB_2M_2 type structure, A stands for alkali's, alkaline earth, or rare earth element, B represents transition metal, M symbolizes pnictogen or chalcogen. The $ThCr_2Si_2$ was the early discovered crystal in this group of compounds [3], as a consequence, this family of crystals is generally known as $ThCr_2Si_2$-type. These crystals got considerable attention because of its unusual characteristics such as superconductivity [4], intermediate valence [5], phase transition [6, 7], and different magnetic properties [8, 9].

The experimental results of these crystals established that by applying pressure or changing, the temperature induced first- and second-order phase transitions [10–14]. These phase transitions are related to the changes of the lattice parameters, in particular, the distance of M–M bonds between the layers of BM_4 tetrahedrons. The literature survey of AFe_2As_2 (A = Ba, Sr, Ca, Eu) visualized that they can be turned into superconductors either by applying pressure [15, 16] or by doping [17–19]. In the past years, much effort has been done on the experimental side for this class of compounds, whereas theoretical studies are relatively inadequate. In AB_2M_2, family Pfisterer and Nagorsen [20] for the first time synthesized $SrCu_2As_2$. Singh [21] performed the electronic structure calculation using the linearized augmented plane wave method within the local density approximation (LDA). The calculation exposed that the maximum density of states is covered by s and p states, the sp metal nature; the bands originated from Cu-*d* states nearly −3.0 eV (bellow Fermi level); therefore, $SrCu_2As_2$ was anticipated to be sp-band metals with Cu atoms contain a formal oxidation state of Cu^{+1} and chemically inert and nonmagnetic $3d^{10}$ state. But there was deficiency of other properties. Anand et al. [22], re-synthesized single crystals of Cu-based compounds $BaCu_2Sb_2$, $SrCu_2As_2$, $SrCu_2Sb_2$ and measure the structural, electronic, magnetic, and transport properties up to 300 K. They observed no phase transition in this range of temperature. Yan et al. [1] synthesized $SrFe_{2-x}Cu_xAs_2$ single crystals and calculate the structural, magnetic, and electronic transport properties. In $SrCu_2As_2$ system, the sp-band metallicity with Cu in $3d^{10}$ electronic configuration is consequent to the valence state Cu^{1+}. As compared to $SrCu_2As_2$, the almost unchanged Cu-2p core line position in $SrFe_{2-x}Cu_xAs_2$ indicates that partial Cu substitutions for Fe in $SrFe_2As_2$ may result in hole doping rather than the expected electron doping. No superconductivity is induced by Cu substitution on Fe sites, even though the structural/spin density wave transition is gradually suppressed with increasing Cu doping [1].

Recently Lv et al. [23] calculated the thermal and elastic properties of $SrCu_2As_2$ by using CASTEP code [24] within generalized gradient approximation, adopted with Wu-Cohen (WC-GGA) [25] and norm-conserving pseudopotential.

Until now, no study in the literature has been found on optical properties for $SrCu_2X_2$ (X = As, Sb) compounds. Therefore, it has been thought of interest to study the optical properties of $SrCu_2X_2$ (X = As, Sb) compounds in addition to electronic structure. In this paper, full potential linear augmented plane wave (FPLAPW) method, have been used to calculate the density of states, electronic band structure, Fermi surface, and optical properties. The FPLAPW method has been proven to be one of the most accurate and flexible method, at reasonable computational expense [26, 27]. This method works with a true crystal

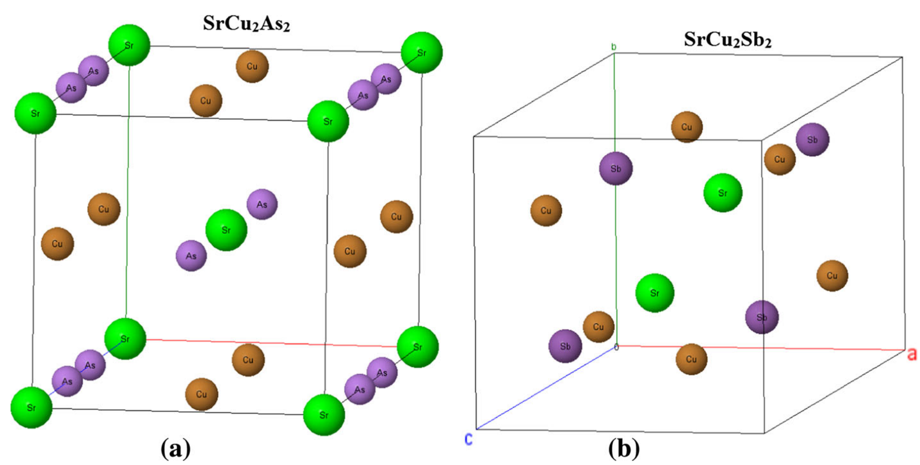

Fig. 1 Optimize unit cell of; **a** $SrCu_2As_2$, **b** $SrCu_2Sb_2$

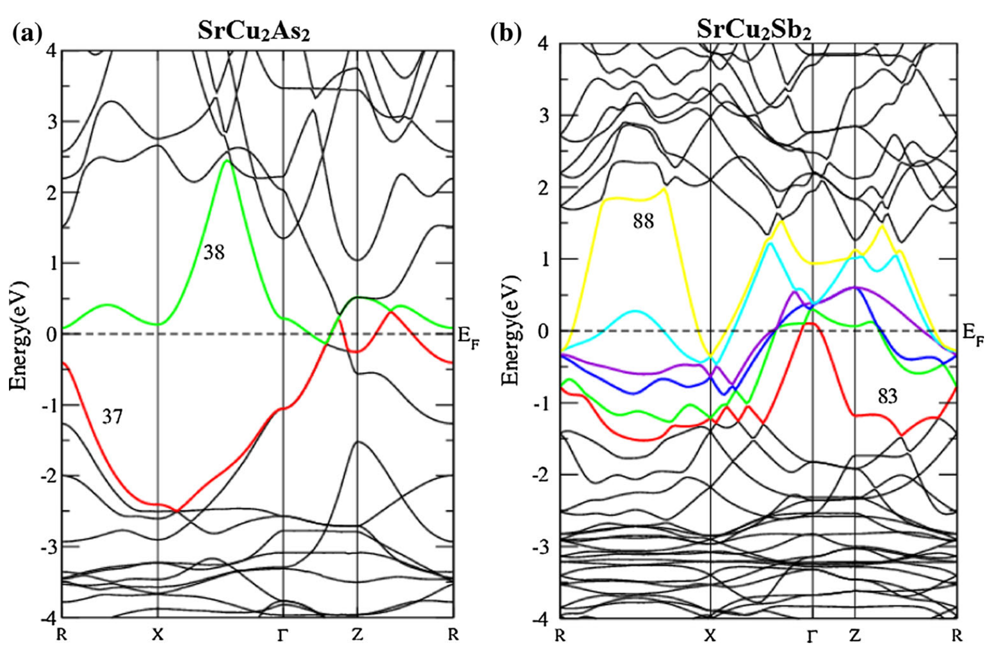

Fig. 2 Calculated band structure of: **a** $SrCu_2As_2$, **b** $SrCu_2Sb_2$

potential, which diverges as at the nucleus, as opposed to the pseudo-potential, in which the singularity is removed [28].

Crystal structure and computational details

In the present calculation, the crystallographic data of $SrCu_2X_2$ (X = As, Sb) are taken from Ref. [22]. The crystal structure of $SrCu_2As_2$ is stable in the body-centered tetragonal structure (*I*4 /mmm), while $SrCu_2Sb_2$ shows the stability in the primitive tetragonal structure (*P*4/nmm), as shown in Fig. 1a, b. The ground state calculations were carried out using full potential linear augmented plane wave (FPLAPW) as implemented in WIEN2k package [29]. The Engel Voskov generalized gradient approximation (EVGGA) [29] was used for calculating the electronic structure and optical properties. Generally, EVGGA obtained by optimizing the exchange–correlation potential V_{xc} as an alternative of the corresponding energy E_{xc} [30]. This scheme yields better band splitting and structural properties that essentially depend on the correctness of the

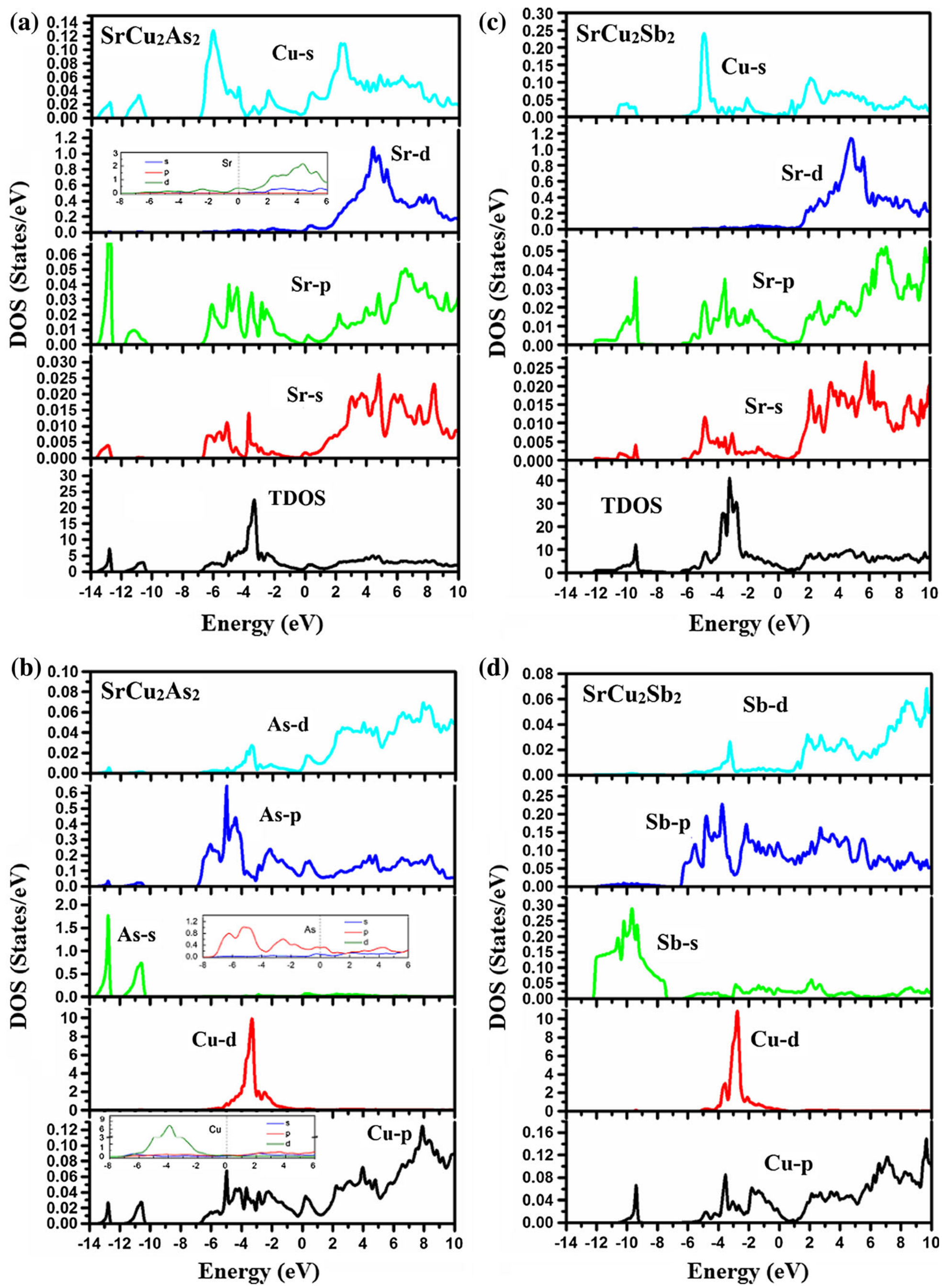

Fig. 3 Calculated total and partial densities of states for: **a** $SrCu_2As_2$, **b** $SrCu_2Sb_2$

exchange–correlation potential [31, 32]. During the calculation, we consider valence electrons corresponding to Sr $5s^2$, Cu $3d^{10}4s^1$, As $3d^{10}$ $4s^2$ $4p^3$, and Sb $4d^{10}$ $5s^2$ $5p^3$ electronic configurations.

The calculations are converged with minimum energy cutoff $R_{MT}K_{max}$up to 7.0 corresponding to 1379 and 3245 plane waves for $SrCu_2As_2$ and $SrCu_2Sb_2$, respectively, where R_{MT} and K_{max} correspond to muffin-tin (MT) sphere radius and magnitude of the largest K vector in plane wave expansion. The selected R_{MT} is 2.0 atomic units (a.u.) for Sr, Cu, As, and Sb in both $SrCu_2As_2$ and $SrCu_2Sb_2$. The wave function inside the sphere was expended up to $l_{max} = 10$, whereas the Fourier expansion of the charge density was $G_{max} = 12(\text{a.u.})^{-1}$ for $SrCu_2As_2$ and $SrCu_2Sb_2$. The valence and core bands are separated by -6.0Ryd. The self-consistent calculations are converged within the difference in total energy of the crystal did not exceed 10^{-2}*mRyd* for succeeding steps. The self-consistent calculations were obtained by using 159 and 144 k points in the irreducible Brillouin zone (IBZ) for $SrCu_2As_2$ and $SrCu_2Sb_2$ compounds.

Result and discussion

Band structure and Fermi surface

The calculated electronic band structure of $SrCu_2X_2$ (X = As, Sb) compounds along the high symmetry points of BZ is shown in Fig. 2a, b. The high dispersion of calculated bands structures around the Fermi level shows high mobility of the charge carrier (heavy hole, light hole, electron) as compared to the low-lying bands. The valence and conduction bands cut the Fermi level confirming the metallic nature of both the compounds.

The calculated total density of states (TDOS) along with partial density of state (PDOS) for $SrCu_2X_2$ (X = As, Sb) compounds is shown in Fig. 3a–d. Our calculated density of states of $SrCu_2As_2$ compound shows good agreement with the previous theoretical work [23]. In $SrCu_2As_2$ compound, we notice that at around −13.0 eV, Sr-*s*, Cu-*s*/*p*, and As-*s*/*p*/*d* states are strongly contributed in bands formation. When we replaced As atom by Sb, one can see that the peaks of Sr-*s*/*p* and Cu-*s*/*p* states around −13.0 eV in $SrCu_2As_2$ compound are vanished, and a small Sr-*s* peak appeared between −11.0 and −9.0 eV in the PDOS of $SrCu_2Sb_2$ compound, while the small peak of Sr-*p* between −12.0 and −10.0 eV in $SrCu_2As_2$ becomes pronounced in $SrCu_2Sb_2$. In addition to that the whole structure of Sr-*s*/*p*/*d* and Cu-*s*/*p* states in $SrCu_2Sb_2$ shifts toward higher energies by 1.0 eV with respect to that of $SrCu_2As_2$.

The density of states around Fermi level [$N(E_F)$] in $SrCu_2As_2$ compound is formed by As-*p*/*d*, Sr-*s*, and Cu-*s* states while for $SrCu_2Sb_2$, compound is formed by Sb-*p*/*d*, Sr-*s*, and Cu-*s* states. The calculated values of $N(E_F)$ are 14.2 states/Ryd-cell and 42.57 states/Ryd-cell for $SrCu_2As_2$ and $SrCu_2Sb_2$ compounds, which show that the metallic nature of $SrCu_2Sb_2$ is three times more that that of $SrCu_2As_2$. The electronic specific heat (γ) is a function of $N(E_F)$ can be determined by using the expression [33]:

$$\gamma = \frac{1}{3}\pi^2 N(E_F) k_B^2, \tag{1}$$

where k_B represents Boltzman constant. The calculated values of γ are 2.60 mJ/mol K^2 (7.37 mJ/mol K^2) for $SrCu_2As_2$ ($SrCu_2Sb_2$) compounds, which confirm our previous observation that the metallic nature of $SrCu_2Sb_2$ is three times greater than that of $SrCu_2As_2$. The calculated value of γ for $SrCu_2As_2$ shows close agreement to the experimental value (2.22 mJ/mol K^2) [22].

Finally, the energy region extended from 1.0 to 10.0 eV, for $SrCu_2As_2$ compound is shaped by Sr-*s*/*d*, Cu-*s*/*p*, and As-*s*/*p*/*d* states, whereas for $SrCu_2Sb_2$, it is formed by Sr-*s*/*p*/*d*, Cu*s*/*p* and Sb-*s*/*p*/*d* states.

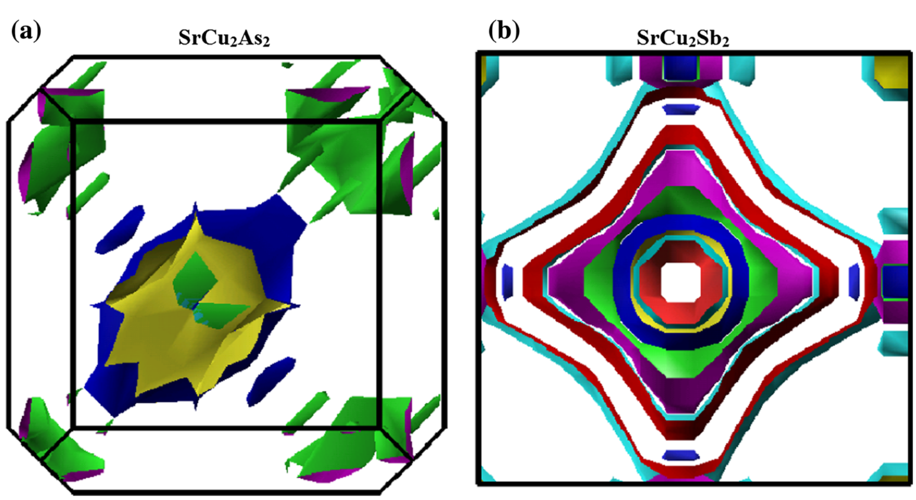

Fig. 4 Calculated Fermi surface for: **a** $SrCu_2As_2$, **b** $SrCu_2Sb_2$

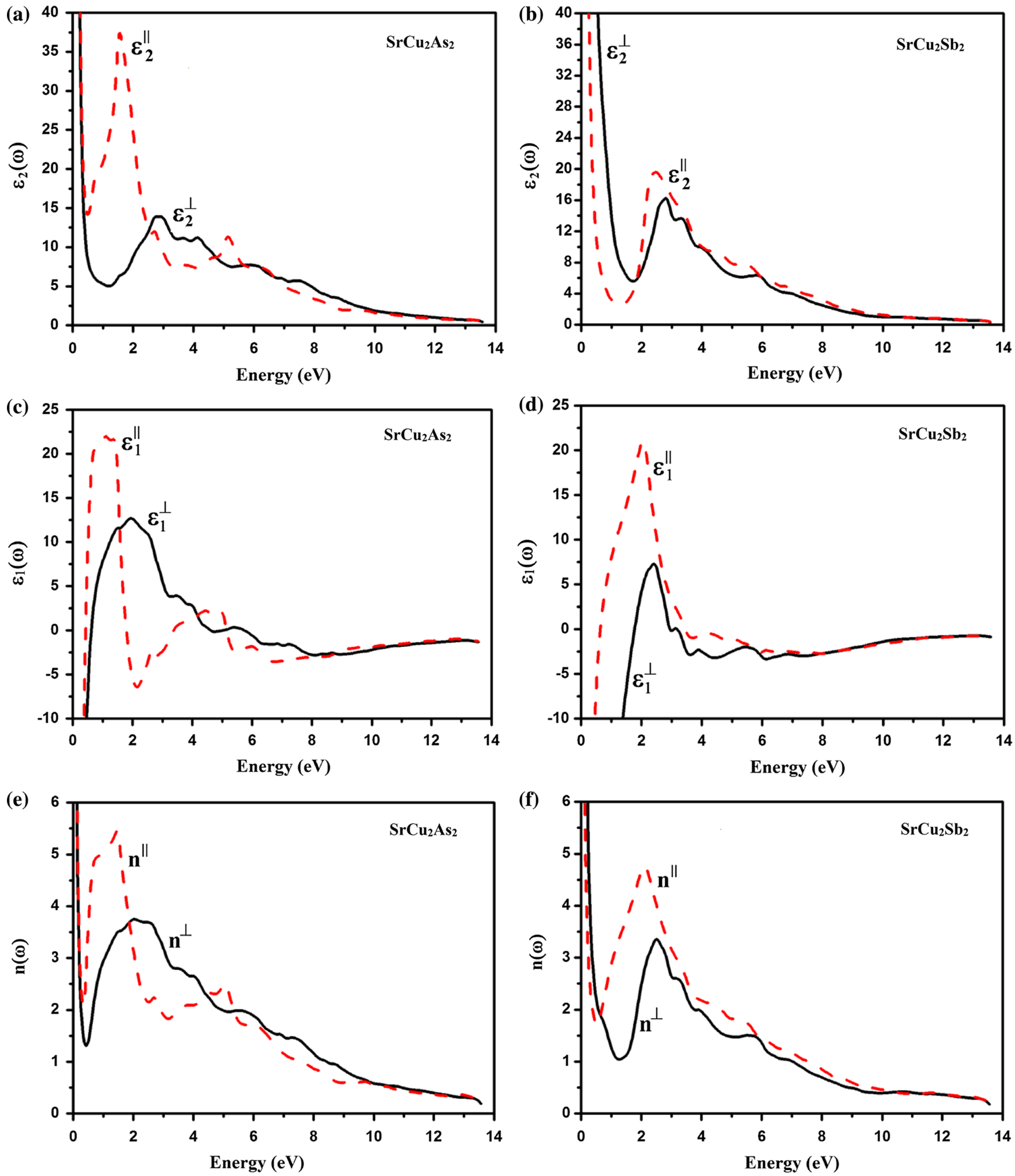

Fig. 5 **a** Calculated imaginary part of dielectric function for $SrCu_2As_2$, **b** Calculated imaginary part of dielectric function for $SrCu_2Sb_2$, **c** Calculated real part of dielectric function for $SrCu_2As_2$, **d** Calculated real part of dielectric function for $SrCu_2Sb_2$, **e** Calculated refractive index of $SrCu_2As_2$, **f** Calculated refractive index of $SrCu_2Sb_2$, **g** Calculated extension coefficient of $SrCu_2As_2$, **h** Calculated extension coefficient of $SrCu_2Sb_2$, **i** Calculated absorption coefficient of $SrCu_2As_2$, **j** Calculated absorption coefficient of $SrCu_2Sb_2$, **k** Calculated reflectivity spectra of $SrCu_2As_2$, **l** Calculated reflectivity spectra of $SrCu_2Sb_2$, **m** Calculated energy loss function of $SrCu_2As_2$, **n** Calculated energy loss function of $SrCu_2Sb_2$, **o** Calculated real part of optical conductivity of $SrCu_2As_2$, **p** Calculated real part of optical conductivity of $SrCu_2Sb_2$, **q** Calculated imaginary part of optical conductivity of $SrCu_2As_2$, **r** Calculated imaginary part of optical conductivity of $SrCu_2Sb_2$

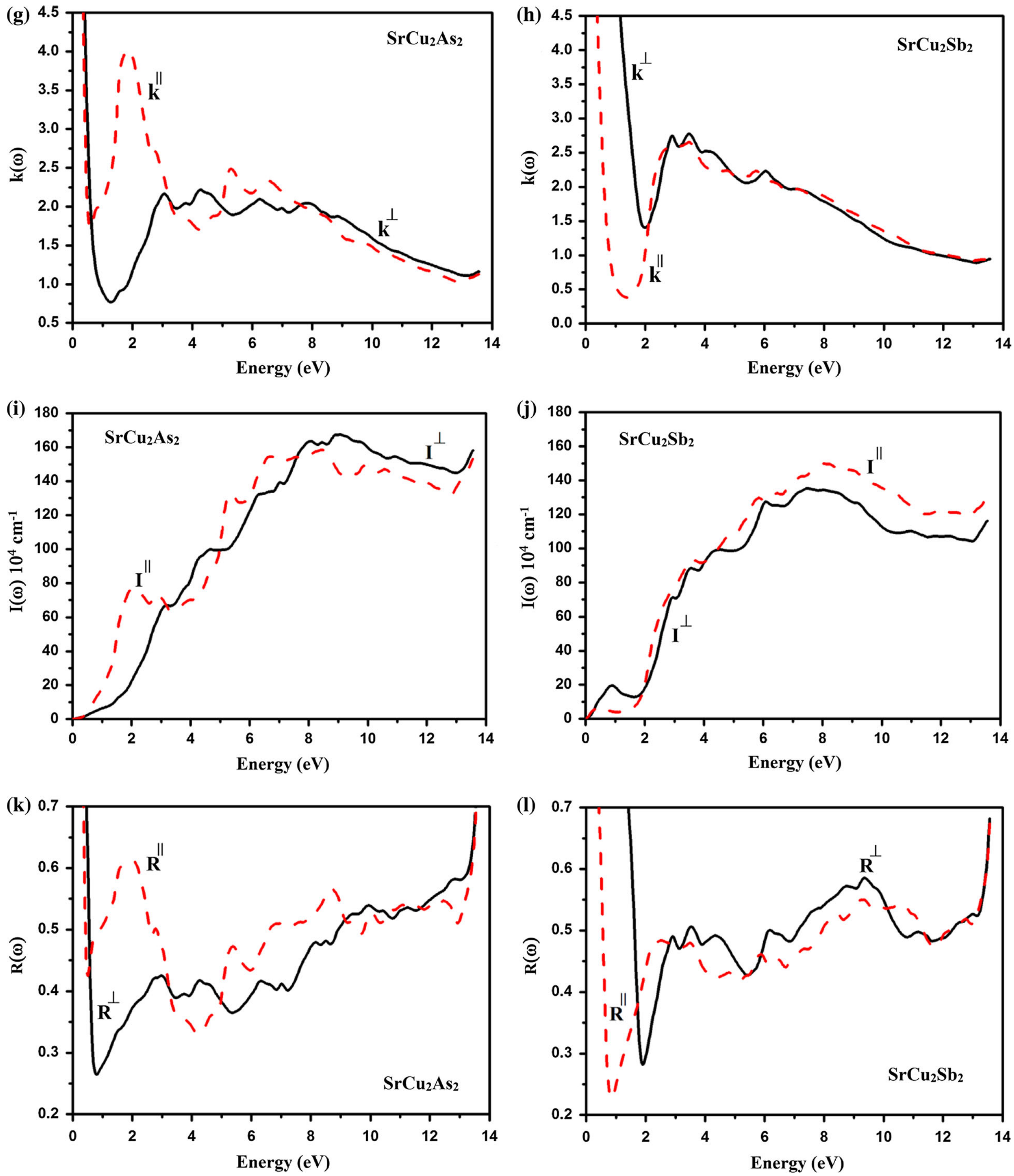

Fig. 5 continued

Figure 4a and b shows the Fermi surface of $SrCu-_2X_2$ (X = As and Sb). For $SrCu-_2As_2$ compounds, the Fermi surface is formed by the bands #37 and 38, while it is formed from the bands #83, 84, 86, 87, and 88 in $SrCu-_2Sb_2$ compound. In the Fermi surface (FS), the white regions represent the hole concentration, while the colors show the presence of electrons [34, 35]. The colors give an idea about the speed of the electrons at Fermi surface, the red color represents the highest speed electrons, the yellow, green, and blue colors exhibit the electrons with intermediate speed, whereas the violet color represents the electrons with the lowest speed [36]. Therefore, from Fig. 4a and b, and due to

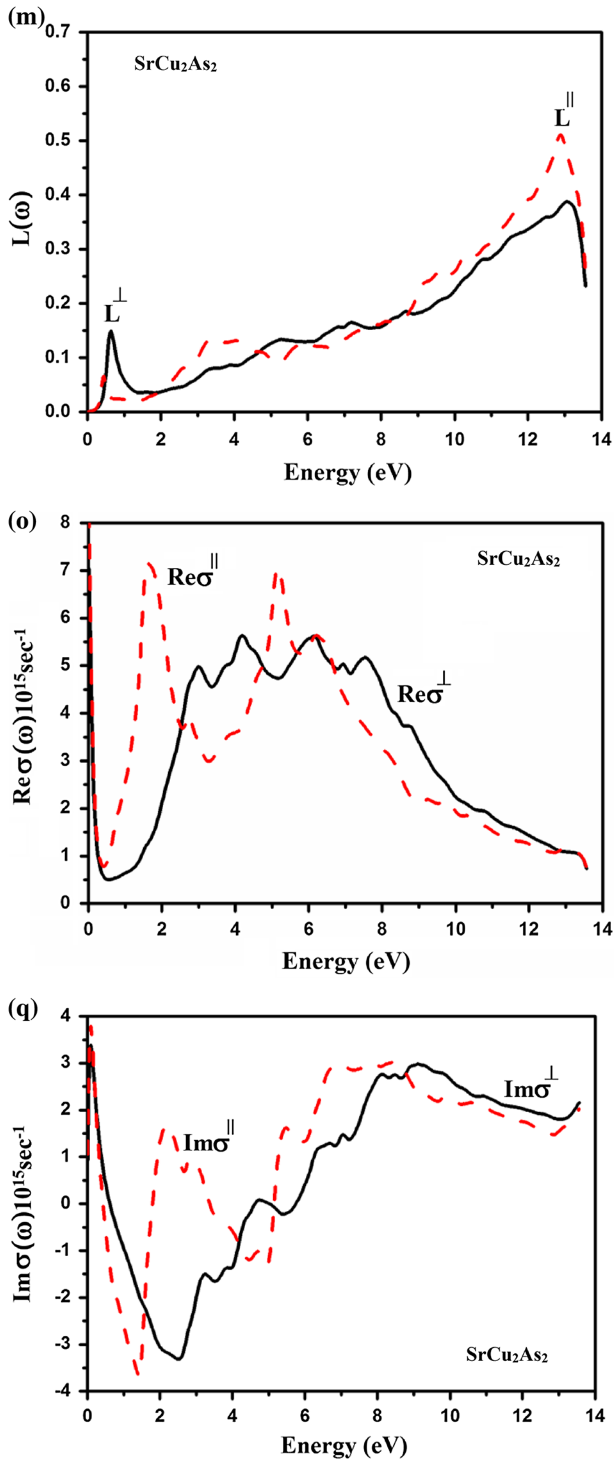

Fig. 5 continued

the colors of FS, one can notice that replacing As by Sb led to increase the metallic nature, which confirms our observation that the metallic nature of $SrCu_2Sb_2$ is greater than that of $SrCu_2As_2$. In general, the transport properties are related to the electrons; these electrons are defined through Fermi surface, which determine the electrical conductivity.

Optical properties

The imaginary part of the frequency dependent dielectric function can be obtained from calculated band structure. The frequency-dependent dielectric function comprises both intra- and inter-band transitions. The intra-band transitions, also known as inter-sub-band transitions, which occur between the quantized level in conduction or valence band are dominant in metals, whereas the inter-band transition occurs between the occupied and unoccupied bands. The correct energy eigenvalues and electron wave functions are necessary to calculate the frequency-dependent dielectric function $\varepsilon(\omega)$. Since the crystal structures of $SrCu_2As_2$ and $SrCu_2Sb_2$ compounds are tetragonal, this symmetry allows only three nonzero dielectric tensor components. These are $\varepsilon_2^{xx}(\omega) = \varepsilon_2^{yy}(\omega)$ and $\varepsilon_2^{zz}(\omega)$, for simplicity, we denote $\varepsilon_2^{xx}(\omega)$ by $\varepsilon_2^{\perp}(\omega)$ and $\varepsilon_2^{zz}(\omega)$ by $\varepsilon_2^{\mathrm{II}}(\omega)$. The imaginary part of the frequency-dependent dielectric function can be calculated using the expression given in Ref. 37:

$$\varepsilon_2^{ij} = \frac{4\pi^2 e^2}{Vm^2\omega^2} \times \sum_{nn'\sigma} \langle kn\sigma | p_i \mid kn'\sigma\rangle\langle kn'\sigma | p_j \mid kn\sigma\rangle \times f_{kn}(1 - f_{kn'})\delta(E_{kn'} - E_{kn} - \hbar\omega), \quad (1)$$

where m and e stand for mass and charge of electron, the symbols ω and V represent the electromagnetic radiation strike the crystal, and unit cell volume, $|kn\sigma\rangle$, describes crystal wave function with crystal momentum k, and σ spin stands for the eigenvalue E_{kn} that corresponds to momentum operator p_j. The Fermi distribution function (f_{kn}) identifies the transition counting from occupied to unoccupied state, and $\delta(E_{kn'} - E_{kn} - \hbar\omega)$ shows the total energy conservation.

Since $SrCu_2X_2$ (X = As, Sb) compounds are metallic, therefore, we must include the Drude term (intra-band transitions) [38]:

$$\varepsilon_2^{\perp}(\omega) = \varepsilon_{2\mathrm{intra}}^{\perp}(\omega) + \varepsilon_{2\mathrm{inter}}^{\perp}(\omega) \quad (3)$$

where

$$\varepsilon_{2\mathrm{intra}}^{\perp}(\omega) = \frac{\omega_p^{\perp 2}\tau}{\omega(1 + \omega^2\tau^2)}. \quad (4)$$

In the expression, τ represents the relaxation time, and $\omega_p^{\perp}$ stands for anisotropic plasma frequency [39]:

$$\omega_p^{\perp 2} = \frac{8\pi}{3}\sum_{kn} v_{kn}^{\perp 2}\delta(\varepsilon_{kn}), \quad (4)$$

where $v_{kn}^{\perp}$ shows electron velocity and ε_{kn} shows the difference between $E_n(k)$ and E_F. Similarly expressions for the parallel component can be written.

Figure 5a and b shows the calculated $\varepsilon_2^{\perp}(\omega)$ and $\varepsilon_2^{\mathrm{II}}(\omega)$ spectra of $SrCu_2As_2$ and $SrCu_2Sb_2$. The sharp rise (<1.0 eV) in the optical spectral structure is due to Drude term [40]. The spectral structures in $\varepsilon_2(\omega)$ (>1.0 eV) are caused by inter-band transitions. The first peak of $SrCu_2As_2$ (>1.0 eV) is formed by the transitions of electrons from bands #35, 36, 37 to band #38, 39, 40. The next peak is originated due to the transitions from band # 32, 33, 34 to band #41, 42, 43 state. Whereas for $SrCu_2Sb_2$, the first peak around 2.5 eV is due to the transitions from band #81, 82 to band #89, and the next peak around 3.4 eV is originated by the transitions from band #79, 80, 81 to band #90, 91, 92. There is a considerable anisotropy between $\varepsilon_2^{\perp}(\omega)$ and $\varepsilon_2^{\mathrm{II}}(\omega)$ for the entire spectral region.

The real part of the dielectric function can be obtained from imaginary part by means of Kramers–Kronig relation [41]:

$$\varepsilon_1(\omega) = 1 + \frac{2}{\pi}P\int_0^{\infty}\frac{\omega'\varepsilon_2(\omega')}{\omega'^2 - \omega^2}d\omega',$$

where P symbolizes the principal value of integral. Figure 5c shows $\varepsilon_2^{\perp}(\omega)$ and $\varepsilon_1^{\mathrm{II}}(\omega)$ of $SrCu_2As_2$ including the Drude term. There exists a considerable anisotropy between the two components from 0.6 to 8.0 eV, and then both components become isotropic. Following Fig. 5c, one can see that the first peaks of $\varepsilon_1^{\mathrm{II}}(\omega)$ occur at 1.0 eV while that of $\varepsilon_2^{\perp}(\omega)$ is situated at 2.0 eV. When we replace As by Sb, the first peak of $\varepsilon_1^{\mathrm{II}}(\omega)$ shifts to be at 2.0 eV and for $\varepsilon_2^{\perp}(\omega)$ at 2.5 eV (Fig. 5d). The two components $\varepsilon_1^{\mathrm{II}}(\omega)$ and $\varepsilon_2^{\perp}(\omega)$ show a considerable anisotropy extended from 0.5 to 7.0 eV.

The other optical constants such as refractive index $n(\omega)$, extension coefficient $k(\omega)$, absorption coefficient $I(\omega)$, reflectivity $R(\omega)$, energy loss function $L(\omega)$, and optical conductivity $\sigma(\omega)$ are shown in Fig. 5e–r. The calculated refractive indices of $SrCu_2As_2$ show considerable anisotropy between $n_2^{\perp}(\omega)$ and $n^{\mathrm{II}}(\omega)$ up to 9.5 eV as illustrated in Fig. 5e. The sharp rise below 1.0 eV is due to intra-band transitions. Then $n^{\mathrm{II}}(\omega)$ forms the first peak at 1.5 eV and $n_2^{\perp}(\omega)$ at 2.0 eV. As we move from As to Sb in the investigated compounds, we notice that the peak of $n^{\mathrm{II}}(\omega)$ shifts to be at 2.25 eV and for $n_2^{\perp}(\omega)$ to be at 2.5 eV with decreasing the peak heights (in Fig. 5f).

The extension coefficient (k) is more significant important phenomena in metals, which shows absorption of energy on surface of the material. The extension coefficient (k) of $SrCu_2As_2$ and $SrCu_2Sb_2$ compounds is presented in Fig. 5g and h. In $SrCu_2As_2$ and $SrCu_2Sb_2$ compounds, both of $k_2^{\perp}(\omega)$ and $k^{\mathrm{II}}(\omega)$ show sharp rise below 1.0 eV which is due to intra-band transitions. In $SrCu_2As_2$ compound At 2.0 eV, $k^{\mathrm{II}}(\omega)$ forms its first peak of about 3.99, while $k^{\perp}(\omega)$ shows broad structure extending between 3.0 and 8.0 eV. Replacing As by Sb causes significant changes in the spectral structure of $k^{\perp}(\omega)$ and $k^{\mathrm{II}}(\omega)$ below 2.0 eV that is attributed to the fact that in $SrCu_2Sb_2$ compound, more bands cut Fermi level, and the value of the density of states at Fermi level is three times greater than that of $SrCu_2As_2$ which makes $SrCu_2Sb_2$ compound more metallic.

The absorption spectra of $SrCu_2As_2$ and $SrCu_2Sb_2$ compounds are shown in Fig. 5i and j. For both compounds, the absorption coefficient increases with increasing the energy to reach the maximum values at 9.0 eV for $SrCu_2As_2$ and at 7.5 eV for $SrCu_2Sb_2$. Further increase of the energy causes to reduce the absorption coefficient.

The reflectivity spectra for both compounds are plotted in Fig. 5k and l; at low energy region, both compounds exhibit sharp rise which is due to intra-band transitions. For $SrCu_2As_2$, $R^{II}(\omega)$forms the first peak at around 2.0 eV, while for $R^{\perp}(\omega)$, the first peak occurs at 2.5 eV. The first valley is formed by $R^{II}(\omega)$ at around 4.0 eV, whereas $R^{\perp}(\omega)$ forms its first valley at 5.5 eV. Then the reflectivity increases with increasing the energy. The reflectivity spectra of $SrCu_2Sb_2$, are illustrated in Fig. 5l; it shows that $R^{II}(\omega)$ forms the first maximum at around 2.5 eV and at 3.5 eV for $R^{\perp}(\omega)$. The first valley occurs at 5.5 eV for both components.

$L(\omega)$ describes the energy loss of fast electron traveling in the material. The two components $L^{\perp}(\omega)$ and $L^{II}(\omega)$ for $SrCu_2As_2$ and $SrCu_2Sb_2$ compounds are illustrated in Fig. 5m and n). The two components are increased with increasing the energy to reach the maximum value at 13.0 eV for both compounds. The sharp peaks produced in $L(\omega)$ are due to the plasma oscillation [42].

The calculated imaginary and real parts of optical conductivity assign response of the material to electromagnetic waves. The optical conductivity $\sigma(\omega)$ is correlated to the dielectric function $\varepsilon(\omega) = 1 + 4\pi i\sigma(\omega)/\omega$. The $\mathrm{Re}\sigma^{II}(\omega)$ spectra of $SrCu_2As_2$ (Fig. 5o) gain the maximum photocurrent at 1.8 eV, and $\mathrm{Re}\sigma^{\perp}(\omega)$ shows maximum value at 4.3 eV. For $SrCu_2Sb_2$ (Fig. 5p), both components show maximum photocurrent at 2.8 eV. The imaginary part of optical conductivity of Fig. 5q and r) is related to the absorptive part of dielectric function (Fig. 5a, b). The $\mathrm{Im}\sigma^{II}(\omega)$ and $\mathrm{Im}\sigma^{\perp}(\omega)$ vary in the same fashion as that of $\varepsilon_2^{II}(\omega)$ and $\varepsilon_2^{\perp}(\omega)$. Both real and imaginary parts of optical conductivity show considerable anisotropy.

Conclusion

We have calculated the electronic band structure density of states, Fermi surface, and optical properties of $SrCu_2X_2$ (X = As, Sb) using all-electron-FPLAPW method within the framework of WIEN2 k. Engel Vosko approximation was used to treat the exchange correlation. The calculated electronic band structure of $SrCu_2Sb_2$ shows more bands cut Fermi level than that of $SrCu_2As_2$. The calculated values of $N(E_F)$ are 14.2 states/Ryd-cell and 42.57 states/Ryd-cell for $SrCu_2As_2$ and $SrCu_2Sb_2$ compounds, which show that the metallic nature of $SrCu_2Sb_2$ is three times more that that of $SrCu_2As_2$. The calculated value of γ for $SrCu_2As_2$ shows close agreement to the experimental value (2.22 mJ/mol K^2) [22]. The optical properties of $SrCu_2As_2$ and $SrCu_2Sb_2$ were calculated. Since these compounds are metallic, therefore, we have included the intra-band transition (Drude term). The spectral peaks of $\varepsilon_2(\omega)$ above 1.0 eV show electron transition from occupied to unoccupied states of the investigated compounds. The other optical constants such as refractive index, extension coefficient, absorption coefficient, reflectivity, energy loss function, and optical conductivity were calculated and discussed in detail. There exists a considerable anisotropy between the two components of all the optical properties of $SrCu_2As_2$ and $SrCu_2Sb_2$.

Acknowledgements The result was developed within the CENTEM project, reg. no. CZ.1.05/2.1.00/03.0088, co-funded by the ERDF as part of the Ministry of Education, Youth and Sports OP RDI programme.

References

1. Yan YJ, Cheng P, Ying JJ, Luo XG, Chen F, Zou HY, Wang AF, Ye GJ, Xiang ZJ, Ma JQ, Chen XH (2013) Structural, magnetic, and electronic transport properties of hole-doped $SrFe_{2-x}Cu_xAs_2$ single crystals. Phys Rev B 87:075105-4
2. Villars P, Calvert LD (1991) Pearson's handbook of crystallographic data for intermetallic phases, 2nd edn. American Society for Metals, Materials Park
3. Ban Z, Sikirica M (1965) The crystal structure of ternary silicides ThM2Si2(M=Cr, Mn, Fe Co, Ni and Cu). Acta Crystallogr 18:594–599
4. Shein IR, Ivanovskii AL (2009) Electronic and structural properties of low-temperature superconductors and ternary pnictides ANi2Pn2 (A=Sr, Ba and Pn=P, As). Phys Rev B 79:054510-7
5. Mörsen E, Mosel BD, Müller-Warmuth W (1988) Mössbauer and magnetic susceptibility investigations of strontium, lanthanum and europium transition metal phosphides with $ThCr_2Si_2$ type structure. J Phys Chem Solids 49:785–795
6. Ronning F, Kurita N, Bauer ED, Scott BL, Park T, Klimczuk T, Movshovich R, Thompson DJ (2008) The first order phase transition and superconductivity in $BaNi_2As_2$ single crystals. J Phys 20:342203–342207
7. Bauer ED, Ronning F, Scott BL, Thompson JD (2008) Superconductivity in SrNi2As2 single crystals. Phys Rev B 78:172504-3
8. Baran S, Bałanda L, Gondek Ł, Hoserd A, Nenkov K, Penca B, Szytuła A (2010) Nature of magnetic phase transitions in $TbCu_2X_2$ (X = Si, Ge) and $HoCu_2Si_2$ compounds. J Alloys Comp. 507:16–20
9. Cabrera-Pasca GA, Carbonari AW, Saxena RN, Bosch-Santos B, Coaquira JAH, Filho JA (2012) Magnetic hyperfine field at highly diluted Ce impurities in the antiferromagnetic compound $GdRh_2Si_2$ studied by perturbed gamma–gamma angular correlation spectroscopy. J Alloys Comp 515:44–48
10. Huhnt C, Michels G, Roepke M, Schlabitz W, Wurth A, Johrendt D, Mewis A (1997) First-order phase transitions in the $ThCr_2Si_2$-type phosphides ARh_2P_2 (A = Sr, Eu). Phys B 240:26–37
11. Huhnt C, Schlabitz W, Wurth A, Mewis A, Reehuis M (1998) First- and second-order phase transitions in ternary europium phosphides with $ThCr_2Si_2$-type structure. Phys B 252:44–54

12. Jesche A, Caroca-Canales N, Rosner H, Borrmann H, Ormeci A, Kasinathan D (2008) Strong coupling between magnetic and structural order parameters in $SrFe_2As_2$. Phys Rev B 78:180504-4
13. Sefat AS, Singh DJ, Jin R, McGuire MA, Sales BC, Mandrus D (2009) Renormalized behavior and proximity of $BaCo_2As_2$ to a magnetic quantum critical point. Phys Rev B 79:024512-5
14. Subedi A, Singh DJ (2008) Density functional study of $BaNi_2As_2$: electronic structure, phonons, and electron-phonon superconductivity. Phys Rev B 78:132511-4
15. Torikachvili MS, Bud'ko SL, Ni N, Canfield PC (2008) Pressure Induced Superconductivity in CaFe2As2. Phys Rev Lett 101: 057006-4
16. Alireza PL, Ko YTC, Gillett J, Petrone CM, Cole JM, Lonzarich GG, Sebastian SE (2009) Superconductivity up to 29 K in $SrFe_2As_2$ and $BaFe_2As_2$ at high pressures. J Phys 21:012208–012212
17. Rotter M, Tegel M, Johrendt D (2008) Superconductivity at 38 K in the iron arsenide $(Ba_{1-x}K_x)Fe_2As_2$. Phys Rev Lett 101: 107006-4
18. Sasmal K, Lv B, Lorenz B, Guloy A, Chen F, Xue Y, Chu CW (2008) Superconducting Fe-based compounds $(A_{1-x}Sr_x)Fe_2As_2$ with A = K and Cs with transition temperatures up to 37 K. Phys Rev Lett 101:107007-4
19. Jeevan HS, Hossain Z, Geibel C, Gegenwart P (2008) High-temperature superconductivity in $Eu_{0.5}K_{0.5}Fe_2As_2$. Phys Rev B 78:092406–092409
20. Pfisterer M, Nagorsen G (1980) On the structure of ternary Arsenides. Z Naturforsch B 35B:703–704
21. Singh DJ (2009) Electronic structure of $BaCu_2As_2$ and $SrCu_2As_2$: *sp*-band metals. Phys Rev B 79:153102–153104
22. Anand VK, Kanchana Perera P, Pandey A, Goetsch RJ, Kreyssig A, Johnston DC (2012) Crystal growth and physical properties of $SrCu_2As_2$, $SrCu_2Sb_2$, and $BaCu_2Sb_2$. Phys Rev B 85:214523–214549
23. Lv ZL, Cheng Y, Chen XR, Ji GF (2013) Electronic, elastic and thermal properties of $SrCu_2As_2$ via first principles calculation. J Alloys Compd 570:156–161
24. Segall MD, Lindan PJD, Probert MJ, Pickard CJ, Harsnip PJ, Clark SJ, Panye MC (2002) First-principles simulation: ideas, illustrations and the CASTEP code. J Phys Condens Matter 14:2717–2744
25. Wu Z, Cohen RE (2006) More accurate generalized gradient approximation for solids. Phys Rev B 73:235116-6
26. Gao S (2003) Linear-scaling parallelization of the WIEN package with MPI. Comput Phys Commun 153:190–198
27. Schwarz K (2003) DFT calculations of solids with LAPW and WIEN2k. J Solid State Chem 176:319–328
28. Grotendorst J, Blügel S, Marx D (2006) Computational nanoscience. NIC Series, Jülich, 31:85–129, ISBN 3-00-017350-1
29. Blaha P, Schwarz K, Madson GKH, Kvasnicka D, Luitz J (2001) WIEN2K, techn. Universitat, Vienna, ISBN 3-9501031-1-1-2
30. Engel E, Vosko SH (1993) Exact exchange-only potentials and the virial relation as microscopic criteria for generalized gradient approximations. Phys Rev B 47:13164–13174
31. Charifi Z, Baaziz H, Reshak AH (2007) Ab-initio investigation of structural, electronic and optical properties for three phases of ZnO compound. Phys Stat Sol B 244:3154–3167
32. Reshak AH, Khan SA (2013) Electronic structure and optical properties of $In_2X_2O_7$ (X = Si, Ge, Sn) from direct to indirect gap: an ab initio study. Comput Mater Sci 78:91–97
33. Reshak AH, Kamarudin H (2011) Theoretical investigation for Li_2CuSb as multifunctional materials: electrode for high capacity rechargeable batteries and novel materials for second harmonic generation. J Alloys Compds 509:7861–7869
34. Reshak AH, Khan SA (2014) Thermoelectric properties, electronic structure and optoelectronic properties of anisotropic $Ba_2Tl_2CuO_6$ single crystal from DFT approach. J Magn Magn Mater 354:216–221
35. Reshak AH, Azam S (2013) First-principles study of the electronic structure, charge density, Fermi surface and optical properties of zintl phases compounds Sr_2ZnA_2 (A = P, As and Sb). J Magn Magn Mater 345:294–303
36. Reshak AH, Azam S (2014) Electronic structure, Fermi surface and optical properties of metallic compound $Be_8(B_{48})B_2$. J Magn Magn Mater 351:98–103
37. Delin A, Ravindran P, Eriksson O, Wills JM (1998) Full-potential optical calculations of lead chalcogenides. Int J Quant Chem 69:349–358
38. Wooten F (1972) Optical properties of solids. Academic press, New York
39. Reshak AH, Azam S (2013) Electronic band structure and specific features of Sm_2NiMnO_6 compound: DFT calculation. J Magn Magn Mater 342:80–86
40. Reshak AH, Charifi Z, Baaziz H (2010) Ab-initio calculation of structural, electronic, and optical characterizations of the intermetallic trialuminides $ScAl_3$ compound. J Solid State Chem 183:1290–1296
41. Tributsch H (1972) Solar energy-assisted electrochemical splitting of water. Z Naturforsch 32A:972–985
42. Marton L (1956) Experiments on low-energy electron scattering and energy losses. Rev Mod Phys 28:172–184